

An optimization-based equilibrium measure describes non-equilibrium steady state dynamics: application to edge of chaos

Junbin Qiu¹ and Haiping Huang^{1,2*}

¹*PMI Lab, School of Physics, Sun Yat-sen University,
Guangzhou 510275, People's Republic of China and*

²*Guangdong Provincial Key Laboratory of Magnetoelectric Physics and Devices,
Sun Yat-sen University, Guangzhou 510275, People's Republic of China*

(Dated: January 19, 2024)

Understanding neural dynamics is a central topic in machine learning, non-linear physics and neuroscience. However, the dynamics is non-linear, stochastic and particularly non-gradient, i.e., the driving force can not be written as gradient of a potential. These features make analytic studies very challenging. The common tool is to use path integral approach or dynamical mean-field theory, but the drawback is one has to solve the integro-differential or dynamical mean-field equations, which is computationally expensive and has no closed form solutions in general. From the aspect of associated Fokker-Planck equation, the steady state solution is generally unknown. Here, we treat searching for the steady state as an optimization problem, and construct an approximate potential closely related to the speed of the dynamics, and find that searching for the ground state of this potential is equivalent to running a stochastic gradient dynamics. The resultant stationary state follows exactly the canonical Boltzmann measure. Within this framework, the quenched disorder intrinsic in the neural networks can be averaged out by applying the replica method. Our theory reproduces the well-known result of edge-of-chaos, and further the order parameters characterizing the continuous transition are derived, and different scaling behavior with respect to inverse temperature in both sides of the transition is also revealed. Our method opens the door to analytically study the steady state landscape of the deterministic or stochastic high dimensional dynamics.

I. INTRODUCTION

Non-equilibrium dynamics is a central topic of statistical physics [1–3], from which general fluctuation-dissipation relations can be established [4–6], and path integral approach was developed to derive the relationship between correlation and response function of the dynamics [7–9]. One benchmark for testing or deriving theoretical hypotheses is the Langevin dynamics with conservative (expressed as gradient of a potential) or nonconservative forces, including Ising spin glass dynamics [10], steady state thermodynamics [11], and neural dynamics with partially symmetric couplings [12]. These studies always resort to dynamical mean-field theory (DMFT) [13, 14], where all possible trajectory paths are integrated to give a physical action, from which correlation and response functions are derived as an optimization of the action [15]. In a general context, the dynamics would be very complicated, e.g., non-gradient and highly coupled, which makes the DMFT very complicated, and even it remains unknown how to capture the steady state properties of these dynamics.

It is commonly observed that the speed of dynamics determines whether the system enters a steady state and thus can be identified [16]. In this paper, we propose a new angle that only the low-speed or zero speed region of the phase space is considered. In this sense, one can write down an energy cost function to optimize for satisfying this speed constraint. This optimization can be formulated under the stochastic gradient dynamics, where a temperature like parameter is introduced. This temperature plays the same role as in the canonical Boltzmann measure. In fact, in the zero temperature and stationary limit, the gradient dynamics are self-consistent with the original general dynamics. Therefore, if the ground state of the energy cost is concentrated on, one can capture the steady state properties of the original phase space. This has an additional benefit that powerful equilibrium concepts such as Boltzmann measure, phase transitions, and order parameters can be leveraged [17].

We verify our framework in recurrent neural networks with asymmetric couplings, where the deterministic dynamics yields order-to-chaos transition [18, 19]. We are able to handle the quenched disorder due to the coupling statistics with the help of replica method, a powerful trick in spin glass theory [20]. Furthermore, two types of order parameters are derived; one describes the network activity, while the other describes the response property of the dynamic system. The former order parameter exhibits a continuous phase transition from null to positive value as the network

*Electronic address: huanghp7@mail.sysu.edu.cn

parameters are tuned, while the latter one shows a peak at the exact location of transition, thereby offering rich physical information about the steady state of the complicated non-gradient dynamics. Different scaling behavior with increasing inverse temperature was found on both sides of the transition point. Our framework also opens the door to analytically study the quasi-potential landscape of a general dynamics, using large-deviation principle and landscape analysis in equilibrium statistical mechanics [17, 21], which is left for a future work.

Our approximate potential analysis is not restricted to simple type of dynamics, and can be generalized to treat competition dynamics of many species in ecosystems [22–24], high-dimensional dynamics of random optimization [25, 26], high-dimensional gradient flow in machine learning [27], and adaptive, hierarchical and noisy neural dynamics in neuroscience [28–32], as long as the dynamics speed can be identified and the steady state exists. The only limitation is that transient behavior before the steady state is reached could not be captured by our equilibrium approximation, and in that case, integro-differential equations are required to solve with expensive computational cost [15]. We next show how physical insights about a complicated non-gradient dynamics can be derived using our approximate potential analysis.

II. MODEL

We consider a recurrent neural network (RNN) composed of N interacting neurons, whose architecture is shown in Fig. 1 (a), illustrated as a simple example of $N = 3$. The network activity is described by N real-valued synaptic currents (\mathbf{x}). The connection strength J_{ij} measures the asymmetric impact from neuron j to neuron i . Note that in our model, two neurons do not have to interact with each other equally, i.e. $J_{ij} \neq J_{ji}$. In addition, $J_{ii} = 0$. All neurons are connected to each other. The synaptic currents are transferred to firing rates through the current-to-rate transfer function $\phi(\cdot)$. Each neuron integrates neighboring activity via the incoming asymmetric synapses, and therefore the dynamics of the current is expressed as the following first-order non-linear differential equation for all i [18, 33]

$$\frac{dx_i}{dt} = -x_i + \sum_{j=1}^N J_{ij}\phi(x_j), \quad (1)$$

where we consider unit time scale. Unless otherwise stated, $\phi = \tanh$. In this case, the transferred neural activity may become negative, while for biological reality, the non-negative function form should be chosen. But our following analysis is still applicable to this type of non-negative transfer function.

In real neural circuits, J_{ij} may not be identically independently distributed (i.i.d.). We therefore consider the correlated case whose statistics is specified below

$$\langle (J_{ij})^2 \rangle = \frac{g^2}{N}, \quad (2)$$

$$\langle J_{ij}J_{ji} \rangle = \frac{g^2}{N}\gamma, \quad (3)$$

where $g > 0$ is called the gain parameter, which controls the variance of connections, and $\gamma \in [-1, 1]$ controls the degree of connection symmetry. The special cases of $\gamma = 1$ and $\gamma = -1$ correspond to symmetric and anti-symmetric neural networks, respectively, while $\gamma = 0$ corresponds to fully asymmetric networks [18].

The above dynamics model exhibits an order-to-chaos transition [19]. The typical number of fixed points explodes as the synaptic gain exceeds a critical value [34], which can be derived from the rightmost boundary of the asymptotic eigenvalue spectrum of \mathbf{J} [35]. When $g(1 + \gamma) < 1$, the network stays in the trivial fixed-point phase, where all trajectories flow to zero activity stable state. Once $g(1 + \gamma) > 1$, the network activity enters a chaotic phase, where an infinitesimal separation of two trajectories would be eventually amplified, and individual neurons exhibit slow to fast time scales as the network parameters go deep into the chaotic phase. We illustrate the phase diagram in Fig. 1 (b) and show the representative dynamic behaviors of these two phases in Fig. 1 (c).

Intuitively, the phase space is partitioned into different regions of different speeds ($\|\frac{d\mathbf{x}}{dt}\|^2$). We are interested in the zero-speed or low-speed regions [16]. Focusing on the speed landscape, we design the following approximate potential (quasi-potential) of the dynamics,

$$E(\mathbf{x}) = \frac{1}{2} \sum_i \left(-x_i + \sum_{j=1}^N J_{ij}\phi(x_j) \right)^2 + \eta \|\mathbf{x}\|^2, \quad (4)$$

where the first term is the kinetic energy, while the second term is a regularization term constraining the ℓ_2 norm of the network activity. η plays the role of tuning the relative strength with respect to the kinetic energy.

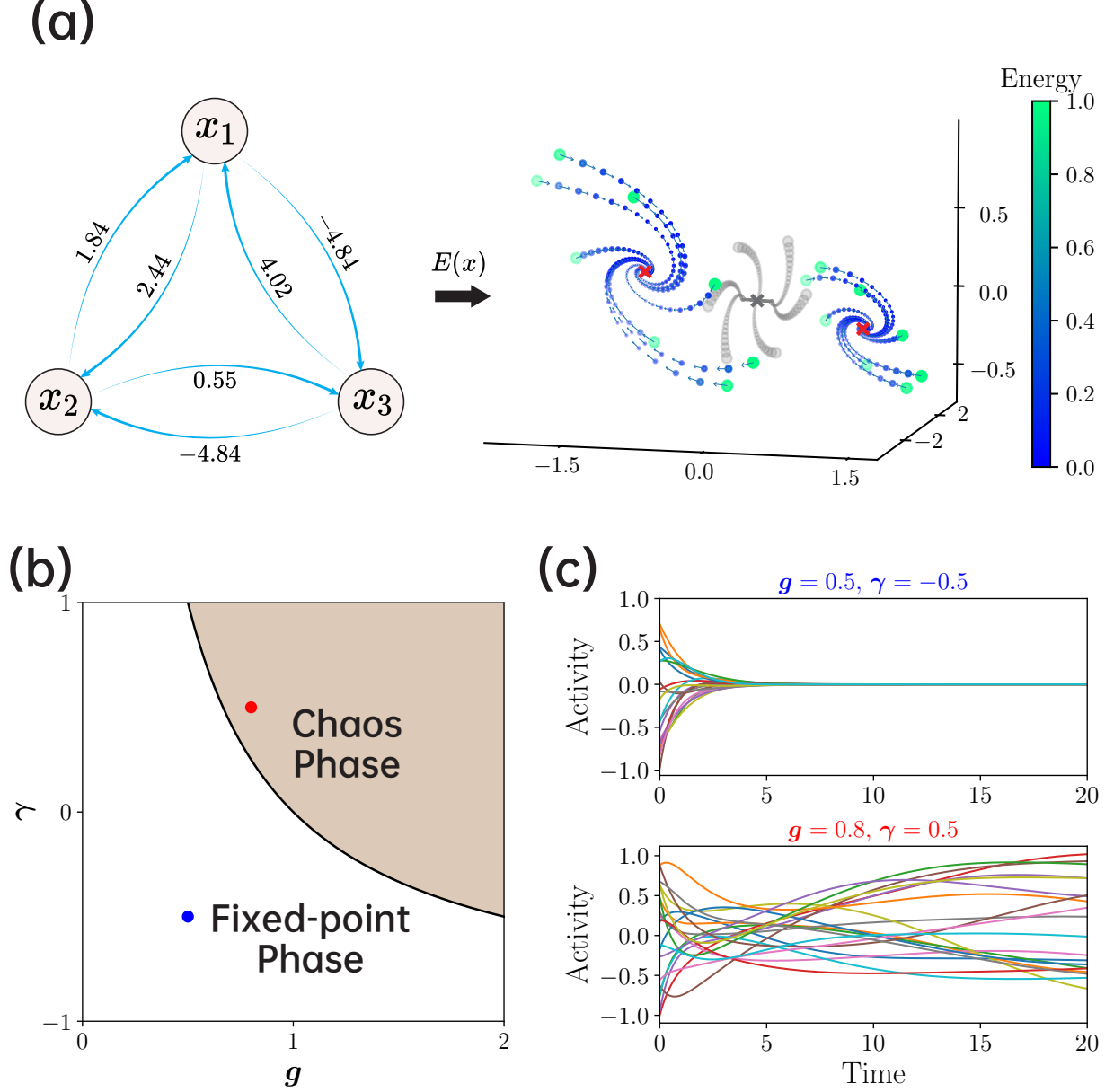


FIG. 1: Key idea of our quasi-potential method and phase diagram of the considered RNN model. (a) A three-neuron recurrent neural network is shown in the left panel. Neurons are bidirectionally connected with the strength displayed near the arrows (synaptic directions). Both connections in opposite directions are correlated once $\gamma \neq 0$. Here, we simulate the RNN dynamics [Eq. (1)], whose phase space displays two fixed points ($g = 1.2, \gamma = 0.1$). In the right panel, we show the trajectories flowing to these fixed points, where the color and size of the dots represent the energy of the corresponding position in the phase space, and the arrows represent the direction and the amount of the velocity (the length of the arrow). We also show an example of the trivial fixed-point for comparison ($g = 0.8, \gamma = 0.1$), where nearby trajectories are shown in the light grey color. The cross symbols denote these corresponding fixed points. (b) The phase diagram as a function of gain parameter g and symmetric degree γ is divided into two regions: null fixed-point and chaotic phases, separated by an analytic transition line $g(1 + \gamma) = 1$ [19]. (c) We show the representative behavior of the dynamics $[\phi(x)]$ in the two phases, corresponding to two colored points in the phase diagram of (b).

According to Eq. (4), we can write down the following stochastic gradient dynamics (or Langevin dynamics)

$$\frac{d\mathbf{x}}{dt} = -\nabla_{\mathbf{x}}E(\mathbf{x}) + \sqrt{2T}\boldsymbol{\epsilon}, \quad (5)$$

where $\boldsymbol{\epsilon}(t)$ is a time-dependent white noise, whose statistics is given by $\langle \epsilon_i(t) \rangle = 0$, $\langle \epsilon_i(t)\epsilon_j(t') \rangle = \delta_{ij}\delta(t-t')$. The temperature T is used to tune the energy level, playing the same role as in the equilibrium Boltzmann measure. We can write the gradient (force) in Eq. (5) in the component wise,

$$F_i \equiv -x_i + h_i - \phi'(x_i) \sum_{j:j \neq i} J_{ji}(h_j - x_j), \quad (6)$$

where $h_i \equiv \sum_{j:j \neq i} J_{ij}\phi(x_j)$. From this expansion, we can see that only in the stationary limit ($T \rightarrow 0$ as well), the above Langevin dynamics closely resembles the original dynamics (the same magnitude order of small speeds). In this sense, the energy defined in Eq. (4) is not a Lyapunov function whose analytic form for the current out-of-equilibrium dynamics with asymmetric couplings is unknown, although the driving force is argued to be decomposed into gradient of a potential related to the steady state distribution and a divergent-free curl flux [36]. The decomposition takes into account the probability conservation of neural state evolution. In contrast, we start from an optimization angle that concentrates on the low-speed region of the phase space, and formulate the steady state behavior as the canonical ensemble of stationary fixed points.

It is well-known that the steady state of the above Langevin dynamics has an equilibrium Boltzmann measure [1],

$$P(\mathbf{x}) = \frac{1}{Z} e^{-\beta E(\mathbf{x})}, \quad (7)$$

where the partition function Z depends on particular realizations of \mathbf{J} , and $\beta = 1/T$. An illustration of $E(\mathbf{x})$ is given in Fig. 1 (a). Our main focus is to compute the free energy of this canonical ensemble, and derive the steady state properties of the dynamics model. The theoretical predictions can be confirmed by simulating a discretized Langevin dynamics, assuming the small discretization step as learning rate, akin to a Monte-Carlo simulation. We remark that this equilibrium analysis reproduces the continuous nature of the dynamics transition, more insights and possibility of exploring the speed landscape would be discussed in the remaining sections.

III. REPLICA METHOD

To derive the quenched disorder average of the free energy, we apply the replica method, which is popular in studying theory of spin glasses [20] and statistical mechanics of neural networks [17]. We first write down the following replicated partition function

$$Z^n = \int d\mathbf{x} e^{-\beta \left(\frac{1}{2} \sum_{i,a} (-x_i^a + \sum_j J_{ij} \phi(x_j^a))^2 + \eta \sum_a \|\mathbf{x}^a\|^2 \right)}, \quad (8)$$

where i, a denote the neuron and replica index, respectively. We denote $d\mathbf{x}$ as a shorthand for $\prod_{i=1}^N \prod_{a=1}^n dx_i^a$, where $x_i^a \in \mathbb{R}$. Therefore, $-\beta f = \lim_{n \rightarrow 0} \frac{\ln \langle Z^n \rangle}{Nn}$, where $\langle \cdot \rangle$ denotes the disorder average over \mathbf{J} . The neural dynamics is much faster than the coupling dynamics, which we assume a stationary limit of fixed \mathbf{J} , and thus the quenched disorder average is required. But if both dynamics evolve in similar time scales, an enlarged state space may be considered, and we leave this issue to future works.

In the course of replica analysis (see details in Appendix A), two order parameters are naturally introduced as follows,

$$Q^{ab} = \frac{1}{N} \sum_i \phi(x_i^a) \phi(x_i^b), \quad (9)$$

$$R^{ab} = \frac{1}{N} \sum_i \hat{x}_i^a \phi(x_i^b), \quad (10)$$

where \hat{x}_i^a acts as a response field, whose name is inspired by the analysis using DMFT [15] and explained in the next section. As the first level of approximation, we assume the replica symmetric ansatz to order parameters

$Q^{ab} = q\delta_{ab} + Q(1 - \delta_{ab})$ and $R^{ab} = r\delta_{ab} + R(1 - \delta_{ab})$, whose physical meaning is explained in more details in Appendix A. Under this approximation, the free energy is given by

$$-\beta f = \frac{1}{2}Q\hat{Q} - q\hat{q} + R\hat{R} - r\hat{r} - \ln \sigma + \frac{1}{2}\beta g^2 \gamma (r^2 - R^2) + \int (DuDv) \ln I, \quad (11)$$

where $\sigma \equiv \sqrt{1 + g^2 \beta (q - Q)}$, and \hat{Q} , \hat{q} , \hat{R} and \hat{r} are conjugated order parameters. The integral $I \equiv \int dx e^{\mathcal{H}(x)}$, where

$$\begin{aligned} \mathcal{H}(x) \equiv & -\beta \eta x^2 + \frac{1}{2}(2\hat{q} - \hat{Q})\phi^2(x) \\ & + \left(\sqrt{\frac{g^2 \beta Q \hat{Q} - \hat{R}^2}{g^2 \beta Q}} u + \frac{\hat{R}}{g\sqrt{\beta Q}} v \right) \phi(x) \\ & - \frac{1}{2\sigma^2} \left(g\sqrt{\beta Q} v + (\hat{r} - \hat{R})\phi(x) - \sqrt{\beta x} \right)^2. \end{aligned} \quad (12)$$

In the large N limit, we can use the saddle-point approximation (also called Laplace method) to derive the closed equations the order parameters must obey. Therefore, by setting the derivatives of the replica free energy with respect to the order parameters zero, we obtain the following compact self-consistent equations (see Appendix B for details)

$$q = [\langle \phi^2 \rangle], \quad (13a)$$

$$Q = [\langle \phi \rangle^2], \quad (13b)$$

$$\hat{q} = -\frac{gk}{2} + \frac{g^2 k^2 Q}{2} + \frac{gk}{2\sigma^2} (\hat{r} - \hat{R}) f(1, 1, -2) [\langle \phi^2 \rangle] \quad (13c)$$

$$+ \frac{gk}{\sigma^2} (\hat{r} - \hat{R}) f(0, -1, 1) [\langle \phi \rangle^2] + \frac{k^2}{2} (1 - 2gkQ) [\langle x^2 \rangle] \quad (13d)$$

$$+ \frac{gk\sqrt{\beta}}{\sigma^2} f(0, 1, -2) [\langle x \rangle \langle \phi \rangle] + \frac{gk\sqrt{\beta}}{\sigma^2} f(-1, 0, 2) [\langle x \phi \rangle] \quad (13e)$$

$$+ gk^3 Q [\langle x \rangle^2], \quad (13f)$$

$$\hat{Q} = g^2 k^2 Q + \frac{2gk}{\sigma^2} (\hat{r} - \hat{R}) f(0, 1, -1) [\langle \phi^2 \rangle] \quad (13g)$$

$$+ \frac{gk}{\sigma^2} (\hat{r} - \hat{R}) f(1, -3, 2) [\langle \phi \rangle^2] - 2gk^3 Q [\langle x^2 \rangle] \quad (13h)$$

$$- \frac{2gk\sqrt{\beta}}{\sigma^2} f(1, -2, 2) [\langle x \rangle \langle \phi \rangle] + \frac{2gk\sqrt{\beta}}{\sigma^2} f(0, -1, 2) [\langle x \phi \rangle] \quad (13i)$$

$$+ k^2 (1 + 2gkQ) [\langle x \rangle^2], \quad (13j)$$

$$r = -\frac{1}{\sigma^2} f(1, 0, -1) [\langle \phi^2 \rangle] + \frac{1}{\sigma^2} f(0, 1, -1) [\langle \phi \rangle^2] \quad (13k)$$

$$+ \frac{\sqrt{\beta}}{\sigma^2} (1 - gkQ) [\langle \phi x \rangle] + \frac{\sqrt{\beta}}{\sigma^2} gkQ [\langle \phi \rangle \langle x \rangle], \quad (13l)$$

$$R = -\frac{1}{\sigma^2} f(0, 1, -1) [\langle \phi^2 \rangle] - \frac{1}{\sigma^2} f(1, -2, 1) [\langle \phi \rangle^2] \quad (13m)$$

$$- \frac{\sqrt{\beta}}{\sigma^2} gkQ [\langle x \phi \rangle] + \frac{\sqrt{\beta}}{\sigma^2} (1 + gkQ) [\langle x \rangle \langle \phi \rangle], \quad (13n)$$

$$\hat{r} = \beta g^2 \gamma r, \quad (13o)$$

$$\hat{R} = \beta g^2 \gamma R, \quad (13p)$$

where $k \equiv \frac{g\beta}{\sigma^2}$ and $f(a, b, c) \equiv a\hat{r} + b\hat{R} + cgkQ(\hat{r} - \hat{R})$. In addition, two kinds of average are specified. One is the disorder average $[\cdot] \equiv \int DuDv \cdot$, and the other is the thermal average $\langle \cdot \rangle \equiv \frac{\int dx e^{\mathcal{H}(x)}}{\int dx e^{\mathcal{H}(x)}}$. $\mathcal{H}(x)$ plays the role of effective Hamiltonian of our model. When $\gamma = 0$ (i.i.d. scenario), \hat{r}, \hat{R} and $f(a, b, c)$ vanish, the above saddle point equation can be greatly simplified (see Appendix C).

IV. RESULTS AND DISCUSSION

A. Equilibrium replica analysis reveals the continuous nature of the chaos transition

The zero temperature limit selects the ground state of the Boltzmann measure [Eq.(7)], which captures the statistics of the steady state solutions of the original non-gradient dynamics [Eq. (1)]. An explicit form of Lyapunov function that is monotonically decreasing over time can only be identified provided that the neural coupling is symmetric, and only in this special case, the Lyapunov function reduces to an Ising-model like Hamiltonian, as encountered in standard Hopfield networks [37]. We thus remark that the quasi-potential defined in Eq. (4) is not the physical potential of the original dynamics, yet capturing only the steady state properties of the dynamics, e.g., the low-(or zero-)speed landscape. In this sense, not all characteristics of a non-gradient dynamics are included in our approximate potential description, e.g., the transient behavior or the temporal evolution of autocorrelation even in the time translation invariant regime is not captured. However, the statistics of fixed-point solutions can be well captured by the quasi-potential approach.

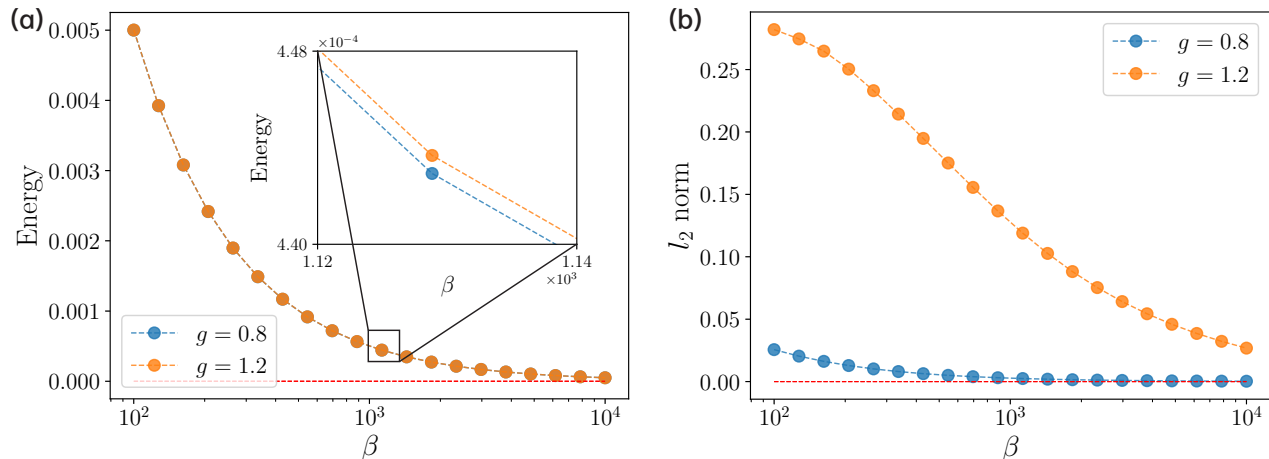


FIG. 2: The average energy (a) and l_2 norm (b) of network activity versus the inverse temperature β in the i.i.d. scenario $\gamma = 0$ with $\eta = 0$. The orange and the blue curves represent the setting $g = 0.8$ and $g = 1.2$, respectively. The red dashed line denotes the ground state energy. Two lines of $g = 0.8$ and $g = 1.2$ are nearly indistinguishable.

The average energy is an indicator of whether the RNN dynamics is trapped in fixed points. In other words, steady states are achievable provided that the average energy can be optimized to the ground state zero value. Without loss of generality, we consider the independent setting $\gamma = 0$ and set $\eta = 0$. As shown in Fig. 2, with increasing value of β , the energy decreases to 0, implying that the ground state can be achieved in a very large β . When $\beta = 10000$, the energy becomes less than 10^{-4} , suggesting that it is reasonable to set $\beta = 10000$ for the zero temperature limit considered in our numerical solutions of the SDEs and experiments verifying our theoretical results. We also show the l_2 norm of the network activity in Fig. 2. The norm displays different magnitudes before and after the onset of chaos.

With a finite temperature, the low-speed solutions of the original dynamics could also be studied. For the remaining analysis, we focus on a very large β (e.g., $\beta = 10^4$) and set $\eta = 0$ unless otherwise stated. Varying the control parameters g and γ , we plot the profiles of all order parameters (q, Q, r, R) in Fig. 3.

Our replica analysis reveals exactly the order-to-chaos transition [19]. When $g < \frac{1}{1+\gamma}$, the zero fixed-point uniquely dominates the phase space, resulting in vanishing q and Q , as expected from the physical definition of the order parameters. Once $g > \frac{1}{1+\gamma}$, q and Q increases rapidly but continually from zero, indicating the emergence of self-sustained collective activity. This coincides with the known picture of exponentially growing topological complexity [34] and the positive maximal Lyapunov exponent [17, 18, 30]. It would be interesting to count the stationary points of our potential, rather than using the hard-to-compute Kac-Rice formula [34], which we left for a future thorough work. Our method thus provides a relatively simple way to access the dynamics landscape in the steady state limit. We remark that the specific form of steady state distribution of the network activity for the original dynamics is unknown.

Let us now look at the associated order parameters involving the response field \hat{x} , which emerges due to the linearization of the quadratic terms in the Hamiltonian (see details in Appendix A). This response field is similar to that used to enforce the dynamics equation in a field-theoretic formula of the stochastic dynamics [15]. But in our

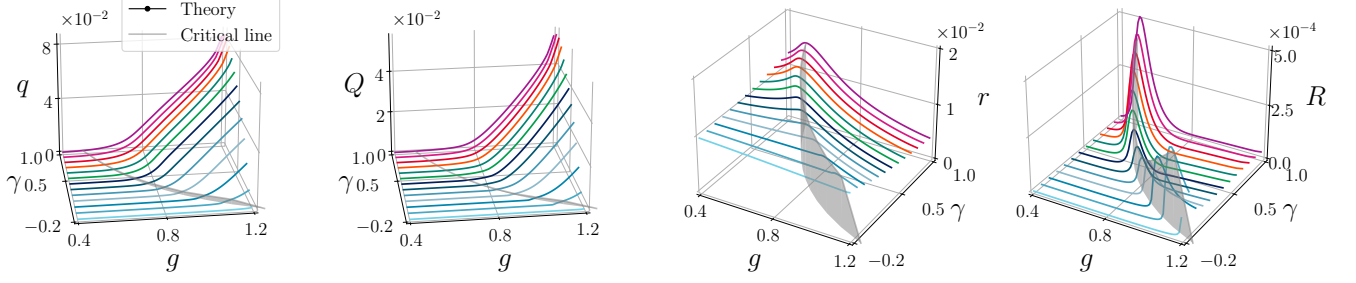


FIG. 3: Order parameter profile as a function of gain parameters g and symmetric degree γ . g is varied from 0.4 to 1.2, and γ is varied from -0.2 to 1.0 with an interval of 0.1 . The colors of curves correspond to the different γ values. The grey vertical plane specifies the location of the critical line $g(\gamma + 1) = 1$ [19].

current setting, the response field is time-independent, as only steady state properties are focused on in this work. Therefore, we argue that R and r bear the same physical meaning with the response function (equal time) in the DMFT language [15]. In fact, r and R display a peak at the transition point. This peak is an indicator of continuous dynamics transition, and may be related to the divergence of the relaxation time-scale of the auto-correlation function [18, 19]. In other words, the dynamics at the edge of chaos is more responsive than at other locations in the phase diagram. The edge of chaos has thus great computational benefits [17, 38, 39]. Surprisingly, this is also consistent with the experimental data of cortical electrodynamics [40], which claimed the information richness at the edge of chaos, and the conscious brain states are observed at the edge of chaos. We conclude that this peak of the response function is a meaningful byproduct of our theory, and moreover an indicator of the edge of chaos.

B. Different scaling behavior of order parameters around the transition

In this section, we investigate how the order parameters behave in the zero temperature limit in a special case of $\gamma = 0$, where the transition point locates at $g = 1$ [18]. The conclusion holds for other values of γ . As shown in Fig. 4, before the onset of chaos ($g = 0.8$), q and Q are inversely proportional to β , as β increases. In addition, \hat{q} and \hat{Q} are proportional to β (either decreasing or increasing). In contrast, after the chaos transition ($g = 1.2$), the large- β asymptotic scaling behavior changes to a different form deviating strongly from that in the case of trivial (ordered) phase. Note that the average energy at $\beta = 10^4$ already converges to zero (the ground state value) (see Fig. 2).

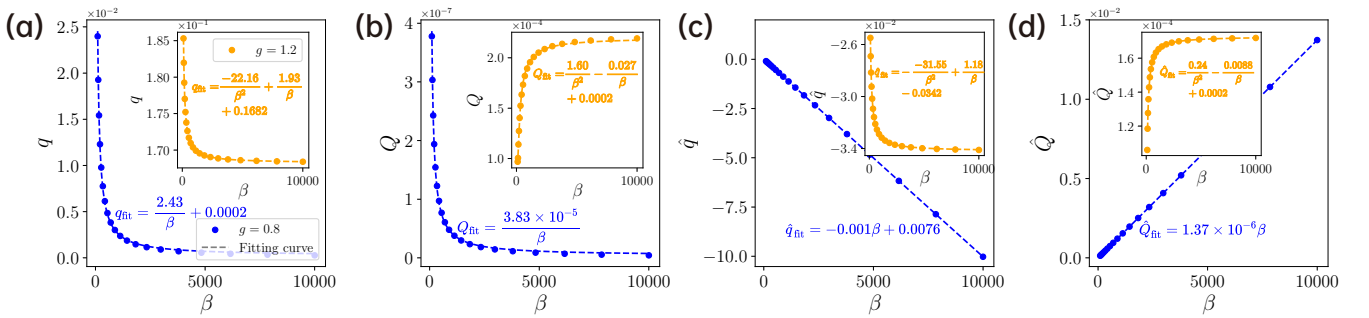


FIG. 4: Order parameters as a function of increasing β . q , Q , \hat{q} and \hat{Q} are plotted in (a), (b), (c) and (d), respectively. We consider $g = 0.8$ (blue dots) in the main figure and $g = 1.2$ (orange dots) in the inset, and tune β from 100 to 10000. The experimental SDE solutions are fitted in an asymptotic form shown in the plots.

V. CONCLUDING REMARKS

In this paper, we provide a relatively simple way to study non-equilibrium dynamics, by proposing a quasi-potential. Under this potential, we derive a stochastic dynamics to implement the optimization of searching for the low-speed region of the phase space. In the zero temperature limit, only the steady states are considered, and thus our canonical ensemble theory yields a good description of the original non-potential dynamics in the long time limit. More precisely, the low (zero)-speed landscape of the phase space can be analytically studied, which is relevant to our mechanistic understanding of recurrent neural dynamics, which can be adaptive, hierarchical and noisy. This equilibrium transformation allows for using the Boltzmann measure to describe the low-speed landscape, as could be derived from the Fokker-Planck equation of the corresponding stochastic dynamics of the optimization [1]. Because of the quenched disorder present in our model, the replica method can be readily adapted as well.

The new finding is that two physically relevant order parameters are derived from our canonical ensemble calculation. One is activity related, which exactly reproduces the order-to-chaos transition phenomenon, previously derived by using more complicated DMFT and random matrix theory [15, 18, 19, 35]. The other is response related, which shows a peak at the very transition point, demonstrating the computation benefits of the edge of chaos. The continuous nature of this chaos transition is confirmed by our theory as well. This transition is related to supersymmetry breaking in a field-theoretic representation of the dynamics in an action [41]. Remarkably, we observe that as the temperature goes to zero, in both sides of the transition point, the order parameters show different scaling behavior with increasing inverse temperature. This is an evidence of dynamical complexity in RNNs.

Our work reveals a quasi-potential landscape behind non-gradient Langevin dynamics (or deterministic dynamics). This could inspire several important future directions. First, a complete picture of this landscape can be studied, as powerful equilibrium approaches can be leveraged, such as large deviation analysis [21], and landscape geometry analysis [42]. Second, one can ask what is the quasi-potential of a coupled-dynamics system where the dynamics of constituent elements can be divided into several levels of different time scales. An enlarged state space is required to introduce. Lastly, one could modify the quasi-potential dynamics to approximate the original non-gradient dynamics with increasing precision.

To sum up, our approach does not rely on the special form of the non-linear dynamics, as long as the speed of the dynamics can be identified, which already includes a broad range of neural dynamics models [17, 28]. Even if the dynamics contains slowly evolving couplings, we can also treat this as a quenched disorder that can be averaged resulting in a self-averaged free energy, from which transitions can be detected and analyzed. As some types of the dynamics can not be accessed by DMFT, or the resultant integro-differential equations for correlation and response functions are hard to solve, our quasi-potential method is a promising starting point to understand the steady state landscape of general non-equilibrium dynamics [43], which includes competition dynamics of many species in ecosystems [22–24], high-dimensional dynamics of random optimization [25, 26], high-dimensional gradient flow in machine learning [27], and adaptive, hierarchical and noisy neural dynamics in neuroscience [28–32].

Appendix A: Details of replica calculation

Starting from Eq. (8), we perform the Hubbard–Stratonovich (HS) transformation $e^{-\frac{1}{2}ab^2} = \int D\hat{x} e^{i\sqrt{ab}\hat{x}}$ for $a > 0$, to linearize the quadratic terms and have

$$Z^n = \int d\mathbf{x} D\hat{\mathbf{x}} \exp \left[i\sqrt{\beta} \sum_{ia} \hat{x}_i^a \left(-x_i^a + \sum_j J_{ij} \phi(x_j^a) \right) - \beta\eta \sum_a \|\mathbf{x}^a\|^2 \right], \quad (\text{A1})$$

where we define $D\hat{x} \equiv e^{-\frac{1}{2}\hat{x}^2} d\hat{x}/\sqrt{2\pi}$ as the Gaussian measure, and we call \hat{x} as a response field [15]. We define i, j as the neuron index and a, b as the replica index. The neuron index runs from 1 to N , while the replica index runs from 1 to n . In addition, $d\mathbf{x} \equiv \prod_{i,a} dx_i^a$ and $D\hat{\mathbf{x}} \equiv \prod_{i,a} D\hat{x}_i^a$.

Before implementation of the quenched disorder average over the coupling statistics, it is convenient to separate the connection matrix into a symmetric part \mathbf{J}^S and an anti-symmetric part \mathbf{J}^A [12],

$$\mathbf{J} = \mathbf{J}^S + \rho \mathbf{J}^A, \quad (\text{A2})$$

where by definition $J_{ij}^S = J_{ji}^S$ and $J_{ij}^A = -J_{ji}^A$, and their variances are defined as follows,

$$\langle (J_{ij}^S)^2 \rangle = \langle (J_{ij}^A)^2 \rangle = \frac{g^2}{N} \frac{1}{1 + \rho^2}. \quad (\text{A3})$$

Both parts are uncorrelated. It then follows that

$$\langle J_{ij} J_{ji} \rangle = \frac{g^2}{N} \frac{1 - \rho^2}{1 + \rho^2} = \frac{g^2}{N} \gamma, \quad (\text{A4})$$

where the relationship between ρ and γ is given below,

$$\rho = \sqrt{\frac{1 - \gamma}{1 + \gamma}}. \quad (\text{A5})$$

Defining $\langle \cdot \rangle$ as the quenched disorder average, we have

$$\langle Z^n \rangle = \int d\mathbf{x} D\hat{\mathbf{x}} \exp \left[-1\sqrt{\beta} \sum_{ia} x_i^a \hat{x}_i^a - \beta\eta \sum_a \|\mathbf{x}^a\|^2 \right] \left\langle \exp \left[1\sqrt{\beta} \sum_{ia} \hat{x}_i^a \sum_j J_{ij} \phi(x_j^a) \right] \right\rangle. \quad (\text{A6})$$

The quenched disorder average is first completed as follows,

$$\begin{aligned} & \left\langle \exp \left[1\sqrt{\beta} \sum_{ij} J_{ij} \sum_a \hat{x}_i^a \phi(x_j^a) \right] \right\rangle \\ &= \left\langle \exp \left[1\sqrt{\beta} \sum_{ij} (J_{ij}^s + \rho J_{ij}^a) \sum_a \hat{x}_i^a \phi(x_j^a) \right] \right\rangle \\ &= \exp \left[-\frac{1}{2} \beta \frac{g^2}{N} \frac{1}{1 + \rho^2} \sum_{i < j} \sum_{ab} \left(\hat{x}_i^a \hat{x}_i^b \phi(x_j^a) \phi(x_j^b) + \hat{x}_i^a \hat{x}_j^b \phi(x_j^a) \phi(x_i^b) + \hat{x}_j^a \hat{x}_i^b \phi(x_i^a) \phi(x_j^b) + \hat{x}_j^a \hat{x}_j^b \phi(x_i^a) \phi(x_i^b) \right) \right] \\ & \quad \times \exp \left[-\frac{1}{2} \beta \frac{g^2}{N} \frac{\rho^2}{1 + \rho^2} \sum_{i < j} \sum_{ab} \left(\hat{x}_i^a \hat{x}_i^b \phi(x_j^a) \phi(x_j^b) - \hat{x}_i^a \hat{x}_j^b \phi(x_j^a) \phi(x_i^b) - \hat{x}_j^a \hat{x}_i^b \phi(x_i^a) \phi(x_j^b) + \hat{x}_j^a \hat{x}_j^b \phi(x_i^a) \phi(x_i^b) \right) \right] \\ &= \exp \left[-\frac{1}{2} \beta \frac{g^2}{N} \sum_{i \neq j} \sum_{ab} \left(\frac{1}{1 + \rho^2} \left(\hat{x}_i^a \hat{x}_i^b \phi(x_j^a) \phi(x_j^b) + \hat{x}_i^a \hat{x}_j^b \phi(x_j^a) \phi(x_i^b) \right) + \frac{\rho^2}{1 + \rho^2} \left(\hat{x}_i^a \hat{x}_i^b \phi(x_j^a) \phi(x_j^b) - \hat{x}_i^a \hat{x}_j^b \phi(x_j^a) \phi(x_i^b) \right) \right) \right] \\ &= \exp \left[-\frac{1}{2} \beta \frac{g^2}{N} \sum_{ij} \sum_{ab} \left(\hat{x}_i^a \hat{x}_i^b \phi(x_j^a) \phi(x_j^b) + \gamma \hat{x}_i^a \hat{x}_j^b \phi(x_j^a) \phi(x_i^b) \right) \right] \\ &= \exp \left[-\frac{1}{2} \beta g^2 \sum_{ab} Q^{ab} \sum_i \hat{x}_i^a \hat{x}_i^b - \frac{1}{2} \beta g^2 N \gamma \sum_{ab} R^{ab} R^{ba} \right], \end{aligned} \quad (\text{A7})$$

where we are left with only γ (whose value can now takes from -1 to 1 , although $\gamma = -1$ is ill-defined for ρ), and we treat in our model the diagonal elements of the connection matrix negligible compared to the contribution from off-diagonal elements of the connection matrix, because of large N limit. To arrive at the last step, we have to introduce the following order parameters

$$Q^{ab} = \frac{1}{N} \sum_i \phi(x_i^a) \phi(x_i^b), \quad (\text{A8})$$

$$R^{ab} = \frac{1}{N} \sum_i \hat{x}_i^a \phi(x_i^b). \quad (\text{A9})$$

Hence, we need to insert the following identity in Eq. (A6),

$$\begin{aligned} 1 &= \prod_{a \leq b} \int dQ^{ab} \delta \left(Q^{ab} - \frac{1}{N} \sum_i \phi(x_i^a) \phi(x_i^b) \right) \prod_{ab} \int dR^{ab} \delta \left(R^{ab} - \frac{1}{N} \sum_i \hat{x}_i^a \phi(x_i^b) \right) \\ &= \int \frac{d\mathbf{Q} d\hat{\mathbf{Q}} d\mathbf{R} d\hat{\mathbf{R}}}{(2\pi)^D} \exp \left[-1 \sum_{a \leq b} Q^{ab} \hat{Q}^{ab} - 1 \sum_{ab} R^{ab} \hat{R}^{ab} + 1 \frac{1}{N} \sum_i \sum_{a \leq b} \hat{Q}^{ab} \phi(x_i^a) \phi(x_i^b) + 1 \frac{1}{N} \sum_{ab} \hat{R}^{ab} \sum_i \hat{x}_i^a \phi(x_i^b) \right] \\ &= \int \frac{d\mathbf{Q} d\hat{\mathbf{Q}} d\mathbf{R} d\hat{\mathbf{R}}}{[2\pi(1/N)^2]^D} \exp \left[-N \sum_{a \leq b} Q^{ab} \hat{Q}^{ab} - N \sum_{ab} R^{ab} \hat{R}^{ab} + \sum_i \sum_{a \leq b} \hat{Q}^{ab} \phi(x_i^a) \phi(x_i^b) + 1 \sum_{ab} \hat{R}^{ab} \sum_i \hat{x}_i^a \phi(x_i^b) \right], \end{aligned} \quad (\text{A10})$$

where $D = n^2 + n(n+1)/2$, and we apply the Fourier transformation of Dirac delta function by introducing the conjugated order parameters \hat{Q}^{ab} , \hat{R}^{ab} , and rescale the order parameters as $\hat{Q}^{ab} \rightarrow -1N\hat{Q}^{ab}$, $R^{ab} \rightarrow -1R^{ab}$ and $\hat{R}^{ab} \rightarrow N\hat{R}^{ab}$ in the last step. $d\mathbf{Q}d\hat{\mathbf{Q}}d\mathbf{R}d\hat{\mathbf{R}}$ is a shorthand for $\prod_{a \leq b} dQ^{ab}d\hat{Q}_{ab} \prod_{ab} dR^{ab}d\hat{R}^{ab}$.

As a result, Eq. (A6) becomes

$$\langle Z^n \rangle \propto \int d\mathbf{x} D\hat{\mathbf{x}} d\mathbf{Q} d\hat{\mathbf{Q}} d\mathbf{R} d\hat{\mathbf{R}} \exp \left[-1\sqrt{\beta} \sum_{ia} x_i^a \hat{x}_i^a - \beta\eta \sum_{ia} (x_i^a)^2 - \frac{1}{2}g^2\beta \sum_{ab} Q^{ab} \left(\sum_i \hat{x}_i^a \hat{x}_i^b \right) + \frac{1}{2}\beta g^2 N\gamma \sum_{ab} R^{ab} R^{ba} \right. \\ \left. - N \sum_{a \leq b} Q^{ab} \hat{Q}^{ab} - N \sum_{ab} R^{ab} \hat{R}^{ab} + \sum_i \sum_{a \leq b} \hat{Q}^{ab} \phi(x_i^a) \phi(x_i^b) + 1 \sum_{ab} \hat{R}^{ab} \sum_i \hat{x}_i^a \phi(x_i^b) \right], \quad (\text{A11})$$

where we have neglected the irrelevant constant due to the variable change in the integral, which does not affect the later saddle point approximation in the large N limit.

Equation (A11) can be rewritten into a compact form,

$$\langle Z^n \rangle \propto \int d\mathbf{Q} d\hat{\mathbf{Q}} d\mathbf{R} d\hat{\mathbf{R}} \exp \left[N \left(- \sum_{a \leq b} Q^{ab} \hat{Q}^{ab} - \sum_{ab} R^{ab} \hat{R}^{ab} + \mathcal{G} \right) \right], \quad (\text{A12})$$

where the model-dependent action \mathcal{G} reads,

$$\mathcal{G} = \ln \int d\mathbf{x} D\hat{\mathbf{x}} \exp \left[-1\sqrt{\beta} \sum_a x^a \hat{x}^a - \beta\eta \sum_a (x^a)^2 - \frac{1}{2}g^2\beta \sum_{ab} Q^{ab} \hat{x}^a \hat{x}^b + \sum_{a \leq b} \hat{Q}^{ab} \phi(x^a) \phi(x^b) \right. \\ \left. + \frac{1}{2}\beta g^2\gamma \sum_{ab} R^{ab} R^{ba} + 1 \sum_{ab} \hat{R}^{ab} \hat{x}^a \phi(x^b) \right], \quad (\text{A13})$$

where $d\mathbf{x}$ and $D\hat{\mathbf{x}}$ have been reduced to $\prod_a dx^a$ and $\prod_a D\hat{x}^a$, respectively.

To proceed, we have to assume the replica symmetric (RS) ansatz as the first level of approximation, i.e., the replica overlap matrix are permutation invariant, as is intuitively expected from the replicated partition function. This first level of approximation can be refined by going to multiple steps of replica symmetry breaking [20], provided that the theoretical prediction is in significant disagreement with numerical simulations. The RS ansatz reads $Q^{ab} = q\delta_{ab} + Q(1 - \delta_{ab})$, $\hat{Q}^{ab} = \hat{q}\delta_{ab} + \hat{Q}(1 - \delta_{ab})$, $R^{ab} = r\delta_{ab} + R(1 - \delta_{ab})$ and $\hat{R}^{ab} = \hat{r}\delta_{ab} + \hat{R}(1 - \delta_{ab})$. We have then the following result of the averaged replicated partition function,

$$\langle Z^n \rangle \propto \int dQ d\hat{Q} dq d\hat{q} dR d\hat{R} dr d\hat{r} \exp \left[N \left(-\frac{n(n-1)}{2} Q\hat{Q} - nq\hat{q} - n(n-1)R\hat{R} - nr\hat{r} + \mathcal{G} \right) \right], \quad (\text{A14})$$

where

$$\mathcal{G} = \ln \int d\mathbf{x} D\hat{\mathbf{x}} \exp \left[-1\sqrt{\beta} \sum_a x^a \hat{x}^a - \beta\eta \sum_a (x^a)^2 + \frac{1}{2}\beta g^2\gamma (n(n-1)R^2 + nr^2) - \frac{1}{2}g^2\beta \left(Q \left(\sum_a \hat{x}^a \right)^2 + (q - Q) \sum_a (\hat{x}^a)^2 \right) \right. \\ \left. + \frac{1}{2} \left(\hat{Q} \left(\sum_a \phi(x^a) \right)^2 + (2\hat{q} - \hat{Q}) \sum_a \phi^2(x^a) \right) + 1 \left(\hat{R} \sum_{ab} \hat{x}^a \phi(x^b) + (\hat{r} - \hat{R}) \sum_a \hat{x}^a \phi(x^a) \right) \right]. \quad (\text{A15})$$

To linearize the quadratic terms in Eq. (A15), we use the HS transformation once again as follows,

$$e^{\frac{1}{2}\hat{Q}(\sum_a \phi(x^a))^2 - \frac{1}{2}g^2\beta Q(\sum_a \hat{x}^a)^2 + 1\hat{R} \sum_{ab} \hat{x}^a \phi(x^b)} = \int Du Dv e^{\kappa_1 u \sum_a \phi(x^a) + v(\kappa_2 \sum_a \phi(x^a) + 1\kappa_3 \sum_a \hat{x}^a)}, \quad (\text{A16})$$

where the auxiliary coefficients $\kappa_1 = \sqrt{\frac{g^2\beta Q\hat{Q} - \hat{R}^2}{g^2\beta Q}}$, $\kappa_2 = \frac{\hat{R}}{g\sqrt{\beta Q}}$ and $\kappa_3 = g\sqrt{\beta Q}$.

Therefore, we have

$$\mathcal{G} = \ln \int Du Dv \exp \left[\frac{1}{2}\beta g^2\gamma (n(n-1)R^2 + nr^2) \right] I^n, \quad (\text{A17})$$

where

$$I \equiv \int dx D\hat{x} \exp \left[-\beta\eta x^2 - \sqrt{\beta}x\hat{x} - \frac{1}{2}g^2\beta(q-Q)\hat{x}^2 + \frac{1}{2}(2\hat{q}-\hat{Q})\phi^2(x) + (\hat{r}-\hat{R})\hat{x}\phi(x) + \kappa_3v\hat{x} + (\kappa_1u + \kappa_2v)\phi(x) \right]. \quad (\text{A18})$$

We next complete the integral over $D\hat{x}$ as

$$\int D\hat{x} \exp \left[-\frac{1}{2}g^2\beta(q-Q)\hat{x}^2 + i\left(\kappa_3v + (\hat{r}-\hat{R}) - \sqrt{\beta}x\right)\hat{x} \right] = \frac{1}{\sigma} \exp \left[-\frac{1}{2}\frac{1}{\sigma^2}\left(\kappa_3v + (\hat{r}-\hat{R})\phi(x) - \sqrt{\beta}x\right)^2 \right], \quad (\text{A19})$$

where $\sigma \equiv \sqrt{1 + g^2\beta(q-Q)}$. Thus we obtain,

$$\mathcal{G} = -n \ln \sigma + \frac{1}{2}\beta g^2\gamma(n(n-1)R^2 + nr^2) + \ln \int DuDv I^n, \quad (\text{A20})$$

where $I \equiv \int dx e^{\mathcal{H}(x)}$, and

$$\mathcal{H}(x) \equiv -\beta\eta x^2 + \frac{1}{2}(2\hat{q}-\hat{Q})\phi^2(x) + (\kappa_1u + \kappa_2v)\phi(x) - \frac{1}{2}\frac{1}{\sigma^2}\left(\kappa_3v + (\hat{r}-\hat{R})\phi(x) - \sqrt{\beta}x\right)^2, \quad (\text{A21})$$

where $\mathcal{H}(x)$ could be considered as the single-variable effective Hamiltonian of our model, which emerges after the quenched disorder is averaged out.

Finally, we perform the saddle point approximation because of large N , such that $\langle Z^n \rangle \propto \int d\mathcal{O} d\hat{\mathcal{O}} e^{N\Phi(\mathcal{O}, \hat{\mathcal{O}})} \approx e^{N\Phi(\mathcal{O}^*, \hat{\mathcal{O}}^*)}$, where $\mathcal{O} = \{Q, q, R, r\}$ and the superscript $*$ refers to the saddle point value. The free energy can be obtained from the replica trick $-\beta f = \lim_{n \rightarrow 0} \frac{\ln \langle Z^n \rangle}{nN}$, and therefore,

$$-\beta f = \frac{1}{2}Q\hat{Q} - q\hat{q} + R\hat{R} - r\hat{r} - \ln \sigma + \frac{1}{2}\beta g^2\gamma(r^2 - R^2) + \int DuDv \ln I. \quad (\text{A22})$$

Appendix B: Saddle Point Equations

In this section, we omit the superscript $*$ on the order parameters, and derive the self-consistent equations these order parameters must obey, which is the so-called saddle point equations (SDEs). The principle is to optimize the action with respect to the order parameters and their conjugated counterparts. The result is given bellow,

$$q = [\langle \phi^2 \rangle], \quad (\text{B1a})$$

$$Q = [\langle \phi \rangle^2], \quad (\text{B1b})$$

$$r = -\frac{1}{\sigma^2}f(1, 0, -1)[\langle \phi^2 \rangle] + \frac{1}{\sigma^2}f(0, 1, -1)[\langle \phi \rangle^2] + \frac{\sqrt{\beta}}{\sigma^2}(1 - gkQ)[\langle x\phi \rangle] + \frac{\sqrt{\beta}}{\sigma^2}gkQ[\langle x \rangle \langle \phi \rangle], \quad (\text{B1c})$$

$$R = -\frac{1}{\sigma^2}f(0, 1, -1)[\langle \phi^2 \rangle] - \frac{1}{\sigma^2}f(1, -2, 1)[\langle \phi \rangle^2] - \frac{\sqrt{\beta}}{\sigma^2}gkQ[\langle x\phi \rangle] + \frac{\sqrt{\beta}}{\sigma^2}(1 + gkQ)[\langle x \rangle \langle \phi \rangle], \quad (\text{B1d})$$

$$\hat{q} = -\frac{gk}{2} + \frac{g^2k^2Q}{2} + \frac{gk}{2\sigma^2}(\hat{r} - \hat{R})f(1, 1, -2)[\langle \phi^2 \rangle] + \frac{gk}{\sigma^2}(\hat{r} - \hat{R})f(0, -1, 1)[\langle \phi \rangle^2] + \frac{k^2}{2}(1 - 2gkQ)[\langle x^2 \rangle] \quad (\text{B1e})$$

$$+ \frac{gk\sqrt{\beta}}{\sigma^2}f(0, 1, -2)[\langle x \rangle \langle \phi \rangle] + \frac{gk\sqrt{\beta}}{\sigma^2}f(-1, 0, 2)[\langle x\phi \rangle] + gk^3Q[\langle x \rangle^2], \quad (\text{B1f})$$

$$\hat{Q} = g^2k^2Q + \frac{2gk}{\sigma^2}(\hat{r} - \hat{R})f(0, 1, -1)[\langle \phi^2 \rangle] + \frac{gk}{\sigma^2}(\hat{r} - \hat{R})f(1, -3, 2)[\langle \phi \rangle^2] - 2gk^3Q[\langle x^2 \rangle] \quad (\text{B1g})$$

$$- \frac{2gk\sqrt{\beta}}{\sigma^2}f(1, -2, 2)[\langle x \rangle \langle \phi \rangle] + \frac{2gk\sqrt{\beta}}{\sigma^2}f(0, -1, 2)[\langle x\phi \rangle] + k^2(1 + 2gkQ)[\langle x \rangle^2], \quad (\text{B1h})$$

$$\hat{r} = \beta g^2\gamma r, \quad (\text{B1i})$$

$$\hat{R} = \beta g^2\gamma R, \quad (\text{B1j})$$

where $k \equiv \frac{g\beta}{\sigma^2}$ and $f(a, b, c) \equiv a\hat{r} + b\hat{R} + cgkQ(\hat{r} - \hat{R})$, and we define disorder and thermal averages, respectively as follows,

$$[\bullet] \equiv \int DuDv \bullet, \quad (\text{B2})$$

and

$$\langle \bullet \rangle \equiv \frac{\int dx e^{\mathcal{H}(x)} \bullet}{\int dx e^{\mathcal{H}(x)}}. \quad (\text{B3})$$

Note that we use the integral identity $\int Dxxf(x) = \int Dxf'(x)$ to write the above SDEs in the compact form.

We are also interested in the average energy, whose ground state value is related to the speed level of the original dynamics. The thermodynamic relation $\langle E \rangle = \frac{\partial[\beta f]}{\partial\beta}$ is used to derive the following formula,

$$\begin{aligned} U = & \frac{g^2}{2\sigma^2}(q - gkQ(q - Q)) - \frac{1}{2}g^2(r^2 - R^2)\gamma + \frac{1}{2\sigma^2}\left(1 + 2\eta\sigma^2 - gk(q - Q) - \frac{2gkQ}{\sigma^2}\right)[\langle x^2 \rangle] + \frac{gkQ}{\sigma^4}[\langle x \rangle^2] \\ & - \frac{1}{2\sqrt{\beta}\sigma^2}\left(f(1, -1, 0) + \frac{1}{\sigma^2}f(0, 1, -3) + gk(q - Q)f(-2, 1, 1)\right)[\langle x\phi \rangle] \\ & - \frac{1}{2\sqrt{\beta}\sigma^2}\left(\frac{1}{\sigma^2}f(0, -1, 3) + gk(q - Q)f(0, 1, -1)\right)[\langle x \rangle \langle \phi \rangle] \\ & - \frac{1}{2g^2Q\beta^2}\left(\hat{R}^2 + g^2k^2Q(q - Q)(\hat{r} - \hat{R})^2 + f(0, -1, 1)(f(0, 1, 1) - 2g^2k^2Q(q - Q)(\hat{r} - \hat{R}))\right)[\langle \phi^2 \rangle] \\ & + \frac{1}{2g^2Q\beta^2}\left(\hat{R}^2 + f(0, -1, 1)(f(0, 1, 1) - 2g^2k^2Q(q - Q)(\hat{r} - \hat{R}))\right)[\langle \phi \rangle^2]. \end{aligned} \quad (\text{B4})$$

To characterize the average activity level in the neural population, we also derive the ℓ_2 norm of the activity as follows

$$\frac{1}{N} \langle \|\mathbf{x}\|^2 \rangle = -\frac{1}{\beta} \frac{\partial(-\beta f)}{\partial\eta} = [\langle x^2 \rangle]. \quad (\text{B5})$$

Appendix C: Independent case $\gamma = 0$

In the case $\gamma = 0$, all the connection weights are independent and uncorrelated. Hence, the expression of the SDEs gets greatly simplified as

$$q = [\langle \phi^2 \rangle], \quad (\text{C1})$$

$$Q = [\langle \phi \rangle^2], \quad (\text{C2})$$

$$r = \frac{\sqrt{\beta}}{\sigma^2}(1 - gkQ)[\langle x\phi \rangle] + \frac{\sqrt{\beta}}{\sigma^2}gkQ[\langle x \rangle \langle \phi \rangle], \quad (\text{C3})$$

$$R = -\frac{\sqrt{\beta}}{\sigma^2}gkQ[\langle x\phi \rangle] + \frac{\sqrt{\beta}}{\sigma^2}(1 + gkQ)[\langle x \rangle \langle \phi \rangle], \quad (\text{C4})$$

$$\hat{q} = -\frac{gk}{2} + \frac{g^2k^2Q}{2} + \frac{k^2}{2}(1 - 2gkQ)[\langle x^2 \rangle] + gk^3Q[\langle x \rangle^2], \quad (\text{C5})$$

$$\hat{Q} = g^2k^2Q - 2gk^3Q[\langle x^2 \rangle] + k^2(1 + 2gkQ)[\langle x \rangle^2], \quad (\text{C6})$$

$$\hat{r} = 0, \quad (\text{C7})$$

$$\hat{R} = 0. \quad (\text{C8})$$

Because $\hat{r} = \hat{R} = 0$, we have $f(a, b, c) = 0$. The free energy is thus reduced to

$$-\beta f = \frac{1}{2}Q\hat{Q} - q\hat{q} - \ln \sigma - \frac{g^2\beta}{2\sigma^2}Q + \int Du Dv \ln I, \quad (\text{C9})$$

where

$$I \equiv \int dx \exp \left[-\frac{1}{2}\beta \left(\frac{1}{\sigma^2} + 2\eta \right) x^2 + \frac{1}{2} \left(2\hat{q} - \hat{Q} \right) \phi^2(x) + \sqrt{\hat{Q}}u\phi(x) + \frac{g\beta}{\sigma^2}\sqrt{Q}vx \right]. \quad (\text{C10})$$

This free energy does not depend on the order parameters r and R anymore. The average energy also yields the following simple form

$$U = \frac{g^2}{2\sigma^2}(q - gkQ(q - Q)) + \frac{1}{2\sigma^2}\left(1 + 2\eta\sigma^2 - gk(q - Q) - \frac{2gkQ}{\sigma^2}\right)[\langle x^2 \rangle] + \frac{gkQ}{\sigma^4}[\langle x \rangle^2]. \quad (\text{C11})$$

Appendix D: Additional experiment results

To illustrate the phase transition in more details, we choose some curves ($\gamma = 0.2, 0.5, 0.8$) and plot them in the 2-dimension plane (Fig. 5). q and Q are close to zero before the critical point, while growing rapidly after the critical point. r and R achieve their maximum values at the critical point. This is also supported by the iteration dynamics of the SDEs (Fig. 7).

Next we explore the effect of β in optimizing the energy and the order parameters. When g is close to the critical point, we show how q varies with increasing β (see Fig. 6 for $g = 0.98$ and $g = 1.0$). We observe that q converges more rapidly towards zero when g is below the critical value. When g is approaching the critical value from below, the decaying towards zero becomes much slower, signaling a continuous phase transition.

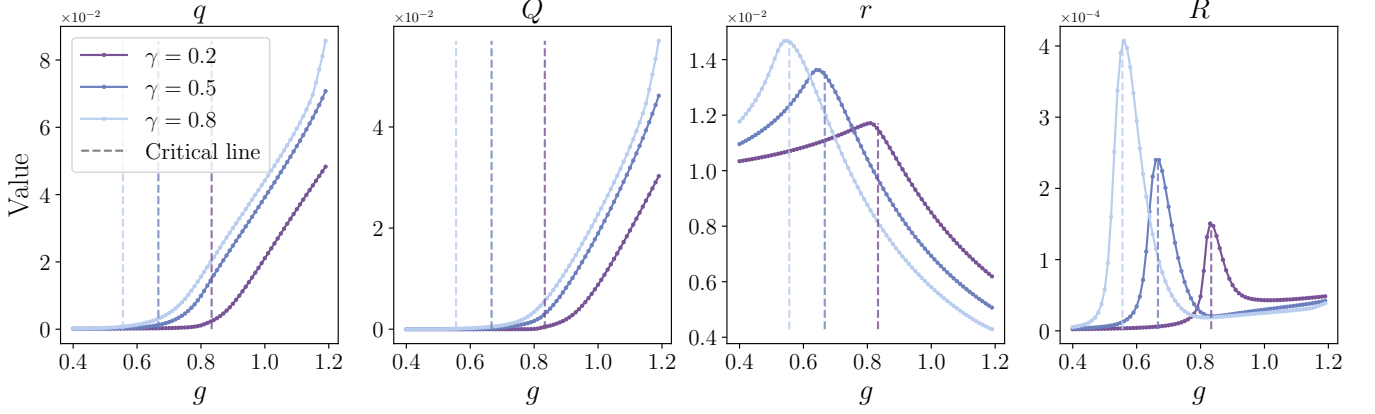


FIG. 5: Phase transitions as g increases. We plot three different curves ($\gamma = 0.2, 0.5, 0.8$), and different colors represent different γ values. The dashed line represents the DMFT result of critical points in Ref. [19].

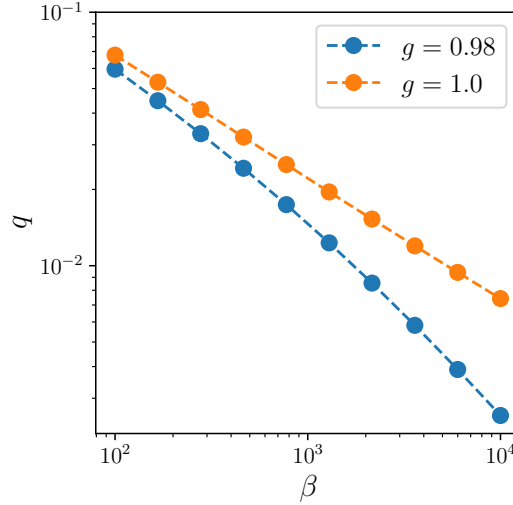


FIG. 6: The relationship between q and β when $g = 0.98$ and $g = 1.0$ ($\gamma = 0$). The blue dots denote $g = 0.98$ case, and the orange dots denote $g = 1.0$. Both axes are in the log scale.

Appendix E: Numerical details of solving SDEs

The most expensive cost of solving SDEs comes from the double average terms, such as $\left[\langle x \rangle^2\right]$ and $\left[\langle \phi \rangle^2\right]$, where the outer integral is related to $DuDv$ and the inner integral is related dx . These integrals are calculated by Monte

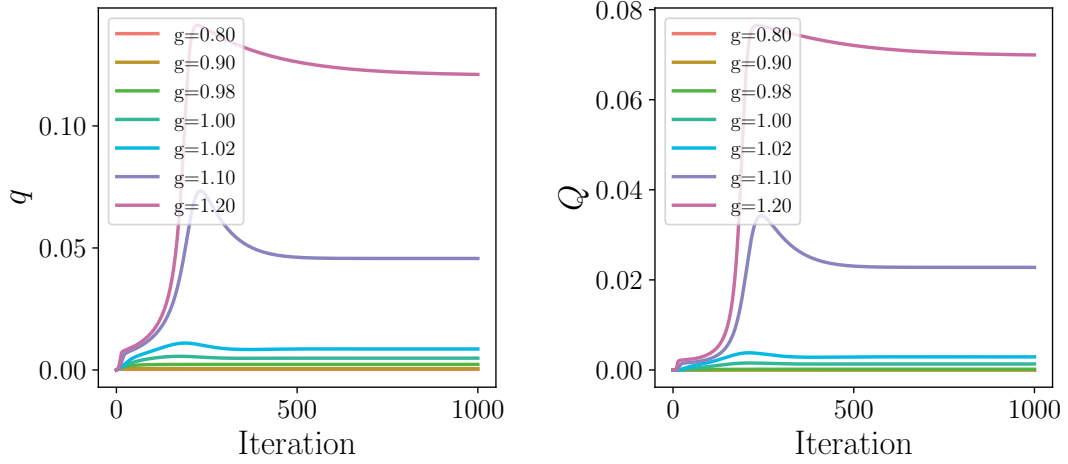


FIG. 7: The iterative dynamics of q and Q for different values of g . All initial values are set to 10^{-5} for q and 10^{-6} for Q . The data points are obtained by using the Algo. 1.

Carlo (MC) method with important sampling technique [17]. Therefore, we need to generate $100k \times 6k$ Gaussian samples, where $100k$ MC samples of u and v is used for the outer integral and $6k$ MC samples of x for each pair of u and v , is used for the inner integral. Note that the inner integral in Eq. (B3) does not contain Gaussian measure at the first sight. However, we can take a reorganization of terms in the effective Hamiltonian. We have then the following equivalent transformation,

$$\langle \bullet \rangle \equiv \frac{\int Dx e^{\tilde{\mathcal{H}}(x)} \bullet}{\int Dx e^{\tilde{\mathcal{H}}(x)}}, \quad (\text{E1})$$

where the Gaussian measure is introduced as $Dx \equiv e^{-\frac{1}{2}\beta(\frac{1}{\sigma^2} + 2\eta)x^2} dx / \sqrt{2\pi}$ and

$$\tilde{\mathcal{H}}(x) \equiv \frac{1}{2}(2\hat{q} - \hat{Q})\phi^2(x) + (\kappa_1 u + \kappa_2 v)\phi(x) - \frac{1}{2} \frac{1}{\sigma^2} (\kappa_3 v + (\hat{r} - \hat{R})\phi(x))^2 + \frac{\sqrt{\beta}}{\sigma^2} (\kappa_3 v + (\hat{r} - \hat{R})\phi(x))x. \quad (\text{E2})$$

After initialization of the order parameters, we complete the double average using the above MC sampling. Then we update the order parameters as follows,

$$\mathcal{O}_{t+1} = \alpha \mathcal{O}_t + (1 - \alpha) f(\mathcal{O}_t), \quad (\text{E3})$$

where α is the damping parameter (a value close to one) to speed up the convergence. $f(\mathcal{O})$ represents the right-hand-side of Eqs. (B1). We stop the iteration when $|\mathcal{O}_{t+1} - \mathcal{O}_t| < 10^{-3}$ for all order parameters. We give a pseudocode in Algorithm. 1 for solving the SDEs.

Algorithm 1 Solver of SDEs

Input: The initial values of order parameters \mathcal{O}_0 , $\mathcal{O} \in \{q, Q, r, R\}$

Output: The convergent values of order parameters \mathcal{O}^*

1: Generate $100k \times 6k$ Gaussian Monte Carlo samples

2: **repeat**

3: Calculate all the double averages by the MC method in Eqs. (B1)

4: Let $\mathcal{O}_{t+1} \leftarrow \alpha \mathcal{O}_t + (1 - \alpha) f(\mathcal{O}_t)$, where $f(\mathcal{O})$ are the functions specified by the SDEs [see Eqs. (B1)]

5: **until** $|\mathcal{O}_{t+1} - \mathcal{O}_t| < 10^{-3}$

6: Let $\mathcal{O}^* \leftarrow \mathcal{O}_t$

Acknowledgments

We would like to thank Zijian Jiang, Yang Zhao and Wenkang Du for helpful discussions at earlier stages of this project. This research was supported by the National Natural Science Foundation of China for Grant Number 12122515

(H.H.), and Guangdong Provincial Key Laboratory of Magnetoelectric Physics and Devices (No. 2022B1212010008), and Guangdong Basic and Applied Basic Research Foundation (Grant No. 2023B1515040023).

-
- [1] Hannes Risken. *The Fokker-Planck Equation: Methods of Solution and Applications*. Springer-Verlag Berlin, Berlin, 1996.
 - [2] Steven H Strogatz. *Nonlinear Dynamics and Chaos: With Applications to Physics, Biology, Chemistry, and Engineering*. CRC Press, 2015.
 - [3] Mikhail I. Rabinovich, Pablo Varona, Allen I. Selverston, and Henry D. I. Abarbanel. Dynamical principles in neuroscience. *Rev. Mod. Phys.*, 78:1213–1265, 2006.
 - [4] Jorge Kurchan. Fluctuation theorem for stochastic dynamics. *Journal of Physics A: Mathematical and General*, 31(16):3719, 1998.
 - [5] Takahiro Ohkuma and Takao Ohta. Fluctuation theorems for non-linear generalized langevin systems. *Journal of Statistical Mechanics: Theory and Experiment*, 2007(10):P10010, 2007.
 - [6] Udo Seifert. Stochastic thermodynamics, fluctuation theorems and molecular machines. *Reports on Progress in Physics*, 75(12):126001, 2012.
 - [7] P. C. Martin, E. D. Siggia, and H. A. Rose. Statistical dynamics of classical systems. *Phys. Rev. A*, 8:423–437, 1973.
 - [8] Hans-Karl Janssen. On a lagrangean for classical field dynamics and renormalization group calculations of dynamical critical properties. *Zeitschrift für Physik B Condensed Matter*, 23(4):377–380, 1976.
 - [9] C. De Dominicis. Dynamics as a substitute for replicas in systems with quenched random impurities. *Phys. Rev. B*, 18:4913–4919, 1978.
 - [10] Hans-Jürgen Sommers. Path-integral approach to ising spin-glass dynamics. *Phys. Rev. Lett.*, 58:1268–1271, 1987.
 - [11] Takahiro Hatano and Shin-ichi Sasa. Steady-state thermodynamics of langevin systems. *Phys. Rev. Lett.*, 86:3463–3466, 2001.
 - [12] A. Crisanti and H. Sompolinsky. Dynamics of spin systems with randomly asymmetric bonds: Langevin dynamics and a spherical model. *Phys. Rev. A*, 36:4922–4939, 1987.
 - [13] Carson C. Chow and Michael A. Buice. Path integral methods for stochastic differential equations. *The Journal of Mathematical Neuroscience (JMN)*, 5(1):8, 2015.
 - [14] John A Hertz, Yasser Roudi, and Peter Sollich. Path integral methods for the dynamics of stochastic and disordered systems. *Journal of Physics A: Mathematical and Theoretical*, 50(3):033001, 2017.
 - [15] Wenxuan Zou and Haiping Huang. Introduction to dynamical mean-field theory of randomly connected neural networks with bidirectionally correlated couplings. *arXiv:2305.08459*, 2023.
 - [16] David Sussillo and Omri Barak. Opening the black box: Low-dimensional dynamics in high-dimensional recurrent neural networks. *Neural Computation*, 25:626–649, 2013.
 - [17] Haiping Huang. *Statistical Mechanics of Neural Networks*. Springer, Singapore, 2022.
 - [18] H. Sompolinsky, A. Crisanti, and H. J. Sommers. Chaos in random neural networks. *Phys. Rev. Lett.*, 61:259–262, 1988.
 - [19] Daniel Marti, Nicolas Brunel, and Srdjan Ostojic. Correlations between synapses in pairs of neurons slow down dynamics in randomly connected neural networks. *Phys. Rev. E*, 97:062314, 2018.
 - [20] M. Mézard, G. Parisi, and M. A. Virasoro. *Spin Glass Theory and Beyond*. World Scientific, Singapore, 1987.
 - [21] Hugo Touchette. The large deviation approach to statistical mechanics. *Physics Reports*, 478(1-3):1–69, 2009.
 - [22] Goel NS, Maitra SC, and Montroll EW. On the volterra and other nonlinear models of interacting populations. *Rev. Mod. Phys.*, 43:231–276, 1971.
 - [23] Robert May. Will a large complex system be stable? *Nature*, 238(5364):413–414, 1972.
 - [24] Yan V. Fyodorov and Boris A. Khoruzhenko. Nonlinear analogue of the may-wigner instability transition. *Proceedings of the National Academy of Sciences*, 113:6827–6832, 2016.
 - [25] Bertrand Lacroix-A-Chez-Toine and Yan V Fyodorov. Counting equilibria in a random non-gradient dynamics with heterogeneous relaxation rates. *Journal of Physics A: Mathematical and Theoretical*, 55(14):144001, 2022.
 - [26] Pierpaolo Vivo. Random linear systems with quadratic constraints: from random matrix theory to replicas and back. *arXiv:2401.03209*, 2024.
 - [27] Max Welling and Yee Whye Teh. Bayesian learning via stochastic gradient langevin dynamics. In *International Conference on Machine Learning*, 2011.
 - [28] Wulfram Gerstner, Werner M. Kistler, Richard Naud, and Liam Paninski. *Neuronal Dynamics: From Single Neurons to Networks and Models of Cognition*. Cambridge University Press, United Kingdom, 2014.
 - [29] Jannis Schuecker, Sven Goedeke, and Moritz Helias. Optimal sequence memory in driven random networks. *Phys. Rev. X*, 8:041029, Nov 2018.
 - [30] M. Helias and D. Dahmen. *Statistical field theory for neural networks*. Springer, Berlin, 2020.
 - [31] David G. Clark, L. F. Abbott, and Ashok Litwin-Kumar. Dimension of activity in random neural networks. *Phys. Rev. Lett.*, 131:118401, 2023.
 - [32] Zijian Jiang, Ziming Chen, Tianqi Hou, and Haiping Huang. Spectrum of non-hermitian deep-hebbian neural networks. *Phys. Rev. Res.*, 5:013090, 2023.
 - [33] Shun-Ichi Amari. Characteristics of random nets of analog neuron-like elements. *IEEE Transactions on Systems, Man, and Cybernetics*, SMC-2(5):643–657, 1972.

- [34] Gilles Wainrib and Jonathan Touboul. Topological and dynamical complexity of random neural networks. *Phys. Rev. Lett.*, 110:118101, 2013.
- [35] H. J. Sommers, A. Crisanti, H. Sompolinsky, and Y. Stein. Spectrum of large random asymmetric matrices. *Phys. Rev. Lett.*, 60:1895–1898, 1988.
- [36] Han Yan, Lei Zhao, Liang Hu, Xidi Wang, Erkang Wang, and Jin Wang. Nonequilibrium landscape theory of neural networks. *Proceedings of the National Academy of Sciences of the United States of America*, 110(45):E4185–E4194, 2013.
- [37] ACC Coolen. Statistical mechanics of recurrent neural networks i—statics. In *Handbook of biological physics*, volume 4, pages 553–618. Elsevier, 2001.
- [38] Chris G. Langton. Computation at the edge of chaos: Phase transitions and emergent computation. *Physica D: Nonlinear Phenomena*, 42(1):12–37, 1990.
- [39] Nils Bertschinger and Thomas Natschläger. Real-time computation at the edge of chaos in recurrent neural networks. *Neural computation*, 16(7):1413–1436, 2004.
- [40] Daniel Toker, Ioannis Pappas, Janna D Lendner, Joel Frohlich, Diego M Mateos, Suresh Muthukumaraswamy, Robin Carhart-Harris, Michelle Paff, Paul M Vespa, Martin M Monti, et al. Consciousness is supported by near-critical slow cortical electrodynamics. *Proceedings of the National Academy of Sciences*, 119(7):e2024455119, 2022.
- [41] G. Parisi and N. Sourlas. Supersymmetric field theories and stochastic differential equations. *Nuclear Physics B*, 206(2):321–332, 1982.
- [42] Haiping Huang and Yoshiyuki Kabashima. Origin of the computational hardness for learning with binary synapses. *Phys. Rev. E*, 90:052813, 2014.
- [43] Haiping Huang. Eight challenges in developing theory of intelligence. *arXiv:2306.11232*, 2023.